RAA 2018 Vol. **18** No. **12**, 150(8pp) doi: 10.1088/1674–4527/18/12/150

http://www.raa-journal.org *http://iopscience.iop.org/raa*

***R**esearch in*
***A**stronomy and*
***A**strophysics*

Long-term optical color behavior of a sample of blazars

Xiao-Pan Li[1], Yu-Hui Luo[1], Hai-Tao Yang[1], Hai-Yan Yang[1], Cheng Yang[2] and Yan Cai[1]

[1] College of Physics and Information Engineering, Zhaotong University, Zhaotong 657000, China; *lxpzrc@163.com*
[2] College of Photoelectron and Communication Engineering, Yunnan Open University, Kunming 650223, China

Received 2018 May 4; accepted 2018 July 4

Abstract We report on the optical color variability of a sample of 24 blazars, consisting of nine flat spectrum radio quasars (FSRQs) and 15 BL Lacertae objects (BL Lacs), on timescales of years using simultaneous V- and R-band observations observed by the Kanata telescope at Higashi-Hiroshima Observatory. The correlations between color indices $V-R$ and magnitudes reveal that 11 BL Lacs and one FSRQ exhibited significant (i.e., $r > 0.2$ and $P < 0.01$) bluer-when-brighter (BWB) trend and two FSRQs followed the redder-when-brighter (RWB) tend, indicating a possibility that the BWB chromatic trend is dominant for BL Lacs and the RWB trend is especially found in FSRQs, which has been presented occasionally in different samples of blazars. The superpositions of the red emission component from the Doppler-boosted relativistic jet and the blue component arising from the accretion disk might be a possible interpretation for the long-term color behaviors.

Key words: galaxies: active — BL Lacertae objects: general — quasars: general — methods: statistical

1 INTRODUCTION

Blazars, an extreme subclass of radio-loud active galactic nuclei (AGNs) with powerful relativistic plasma jets beamed toward us, are characterized by their luminous, rapidly variable and polarized nonthermal continuum emissions across nearly the entire electromagnetic spectrum (e.g., Urry & Padovani 1995). Based on the equivalent width (EW) of the optical broad emission, blazars are subdivided into two subclasses: flat spectrum radio quasars (FSRQs) with strong emission lines and BL Lacertae objects (BL Lacs) which have either very weak (EW$<$5 Å) or no emission lines. The broadband spectral energy distributions (SEDs) of blazars normally exhibit a double-peak structure in the ν–νF_ν representation. The low-energy bump peaks at the infrared (IR)-optical-ultraviolet band, which is explained by synchrotron emission from relativistic electrons in the jet, while the high-energy bump peaks at the MeV–TeV gamma-ray band, which may be due to the inverse Compton (IC) scattering of seed photons by the synchrotron-emitting electrons emitting the synchrotron bump (leptonic models) (e.g., Böttcher 2007), or the alternative hadronic processes (hadronic models) (e.g., Mücke et al. 2003; Böttcher et al. 2013). In the case of leptonic models, the low-energy seed photons could be from local synchrotron radiation on the same relativistic electrons (synchrotron self-Compton; SSC) (e.g., Marscher & Gear 1985) or from an external photon field (external Compton; EC) such as the accretion disk, broad-line region (BLR) or external torus (e.g., Ghisellini & Tavecchio 2009).

Based on the frequencies of synchrotron peaks in the SEDs, blazars can be subdivided into three subclasses: low synchrotron peaked blazars (LSPs; for sources with $\nu^{\rm syn}_{\rm peak} < 10^{14}$ Hz), intermediate synchrotron peaked blazars (ISPs; $10^{14}\,{\rm Hz} < \nu^{\rm syn}_{\rm peak} < 10^{15}\,{\rm Hz}$) and high synchrotron peaked blazars (HSPs; $\nu^{\rm syn}_{\rm peak} > 10^{15}$ Hz) (Abdo et al. 2010). In most cases, FSRQs are found to be LSPs, while BL Lacs are found in all three spectral subclasses. However, FSRQs of LSPs also show some different characteristics from LSP BL Lac objects, such as different optical emission lines and different underlying contributions from the thermal disks, though they have similar positions of the synchrotron peaks (e.g.,

Lister et al. 2011; Bonning et al. 2012; Linford et al. 2012).

Flux variability of blazars has been observed over the entire range of their continuum emission, with various timescales from decades down to hours and minutes. Blazar variabilities can be broadly divided into intraday variability (IDV) or micro-variability with timescales being less than one day, short-term variability (STV) with timescales from days to a few months and long-term variability (LTV) with timescales from several months to years. Generally, the most favored intrinsic models known as shock-in-jet models and the various geometrical effects related to the jet, such as precession and helical structures, are usually proposed to account for the LTV mechanism. Multiwavelength flux research is an important approach to test the size and location of the emitting region at a given frequency, physics of particle processes and radiation mechanisms in the jet. Furthermore, the optical flux variability on long-term timescales provides a way to explore the properties of flux, color and spectral variations, and can be useful in understanding the complex interrelations between emission properties at different frequencies (Marchesini et al. 2016).

Recently, Itoh et al. (2016) presented a large collection of optical–near-IR photometry and polarimetry monitoring of 45 blazars taken in 2008–2014, systematically studying the mechanisms of variability and reporting a systematic difference in the intrinsic alignment of magnetic fields in jets between FSRQs and BL Lacs. In this paper, we further search for the correlation between flux and color variations on long-term timescales with their optical observations to investigate the color behavior of a sample of blazars. We present the properties of the sample, and correlation studies of the flux and color in Sections 2 and 3, respectively. Discussions and conclusions are given in Section 4.

2 SAMPLE SELECTION AND DATA REDUCTION

The photopolarimetry monitoring of these 45 blazars was performed with the 1.5 m Kanata telescope at Higashi-Hiroshima Observatory. Each photopolarimetric observing sequence consisted of successive exposures at four position angles of a half-wave plate: 0°, 45°, 22.5° and 67.5°. The magnitudes were measured using standard aperture photometry procedures and corrected for Galactic extinction. The photometric data of *V*-, *R*-, *J*- and *K*-band and polarimetry of *V*- and *R*-band are available at the VizieR Online Data Catalog[1].

Simultaneous *V*- and *R*-band observations were performed to search for the optical color behavior in this study. However, observational gaps always inevitably occurred in the light curves due to low photon statistics, bad weather, monitoring schedule and maintenance of instruments, which distinctly constrain the selection in the samples. In order to ensure accuracy of the investigation, we only accepted simultaneous *V*- and *R*-band observations with observational interval less than 2 hours (typically 15 mins) to calculate the color index $V - R$. The error of color index was calculated via standard error propagation, i.e., $\sigma_{V-R} = \sqrt{\sigma_V^2 + \sigma_R^2}$. Finally, among 45 blazars, we selected 24 targets which have more than 10 simultaneous *V*- and *R*-band optical data points extending more than 3 months. As summarized in Table 1, we list our sample which comprises nine FSRQs and 15 BL Lacs, or six HSPs, six ISPs and 12 LSPs if considering the SED classification. The time span ΔT for each source is also given.

Figure 1 displays an example of light curves and a color index curve in the samples. One can note that both light curves and the color index curve of OJ 287 show strong activities on diverse timescales, which are common features in blazars.

3 COLOR VARIABILITY ON LONG-TERM TIMESCALES

The variabilities of color indices associated with the spectral variabilities in optical and IR bands give us a clue to investigate the mechanisms of variability in blazars and search for a basic relation between the several subclasses of blazars. In this study, we concentrate on the global correlations between the flux and color variations on long-term timescales for each analyzed sample.

Figure 2 presents the $V - R$ vs. V-band magnitudes for the sample of blazars listed in Table 1, as well as the classification of the sources. For each source, we evaluate the corresponding color–magnitude Pearson correlation coefficient r to quantify general trends in a spectral appearance on long-term timescales. The obtained values of the correlation coefficient r, together with the slope of

[1] *http://vizier.u-strasbg.fr/viz-bin/VizieR?-source=J/ApJ/833/77 http://vizier.u-strasbg.fr/viz-bin/VizieR?-source=J/ApJ/833/77*,CDS, Strasbourg, France. For more details about the Kanata telescope and the standard recipes of photometric data analysis, refer to Itoh et al. (2016), Ikejiri et al. (2011) and references therein.

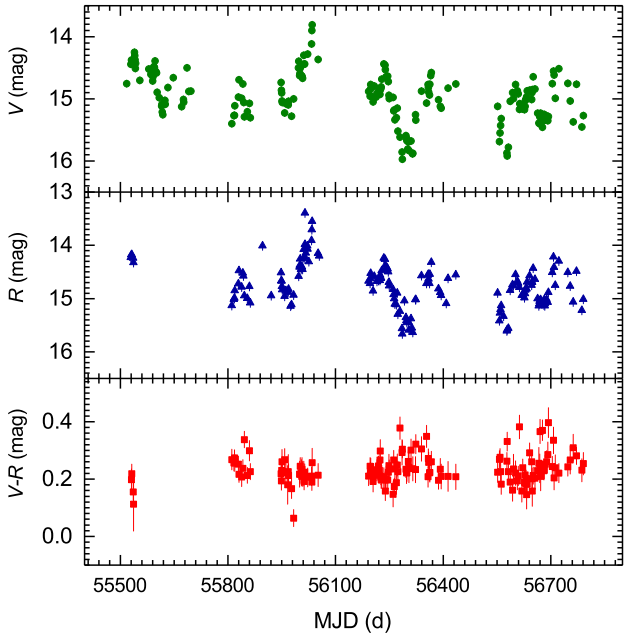

Fig. 1 Example of light curves and color index curve in the samples. The top and middle panels show the *V*- and *R*-band light curves of OJ 287 respectively from November 2010 to May 2014, and the bottom panel displays the corresponding color index curve.

linear regression fitting S, null hypothesis probability P, the number of simultaneous data points N and the corresponding average spectral index $\langle\alpha_{VR}\rangle$, are all given in Table 1 as well. The average spectral indices quoted in Table 1 are derived here simply as (e.g., Wierzcholska et al. 2015; Agarwal & Gupta 2015; Gupta et al. 2017)

$$\langle\alpha_{VR}\rangle = \frac{0.4\langle V-R\rangle}{\log(\nu_{\rm V}/\nu_{\rm R})}\ , \qquad (1)$$

where ν_V and ν_R are the effective frequencies of the respective bands (Bessell et al. 1998) and $\langle V-R\rangle$ is the average color index.

Generally, according to the correlation between color indices and magnitudes, the behavior of blazars can be simply divided into three classes, i.e., colors get bluer when the source tends to be brighter, which is the so called bluer-when-brighter (BWB) trend, colors get redder when the source tends to be brighter, namely the redder-when-brighter (RWB) trend and no clear tendency at all. In our analysis as summarized in Column (9) of Table 1, positive color–magnitude correlations with $r > 0.2$ and $P < 0.01$ indicate that the source appears to exhibit a general BWB trend, while the negative correlations with $r < -0.2$ and $P < 0.01$ mean an RWB trend. In addition, the other cases that have correlations with $P > 0.01$ suggest that no significant correlation between color indices and magnitudes can be derived. These criteria are used in the optical/IR color variability analysis of blazars (Zhang et al. 2015). Furthermore, although different time spans and varying spacings of the Kanata observations caused different time and color scales for different sources, our selection criteria can generally reveal a relatively stable analysis result (e.g., Wierzcholska et al. 2015). Then, the detected color behavior for each source is listed in Table 1, in which a "None" behavior means that no significant BWB/RWB trend was derived.

Overall, in our samples of 24 blazars, we found that 12 blazars, including 11 BL Lacs and one FSRQ (PKS 1749+096), had significant BWB trends on long-term timescales. Only two FSRQs (LSPs), CAT 102 and 3C 454.3, had a negative correlation, in other words, an RWB trend. The other six FSRQs (PKS0454–234, PMN J0948+0022, 3C 273, 3C 279, PKS 1510–089 and 3C 371) and four BL Lacs (PKS 0048–097, 3C 66A, Mrk 501 and 1ES 2344+514) showed no significant correlation between color indices and magnitudes in this campaign. Moreover, if we consider the SED classification, four of six HSPs have a BWB trend, three of six ISPs have a BWB trend, five of 12 LSPs have a BWB trend and two of 12 LSPs have an RWB trend, as listed in Table 1. Notwithstanding, one can note that the LSP PKS 1749+096 shows a significant positive correlation, which mainly comes from the three points with extremely large values of $V-R$. However, after removing the three points, we found that this source, 1749+096, still follows

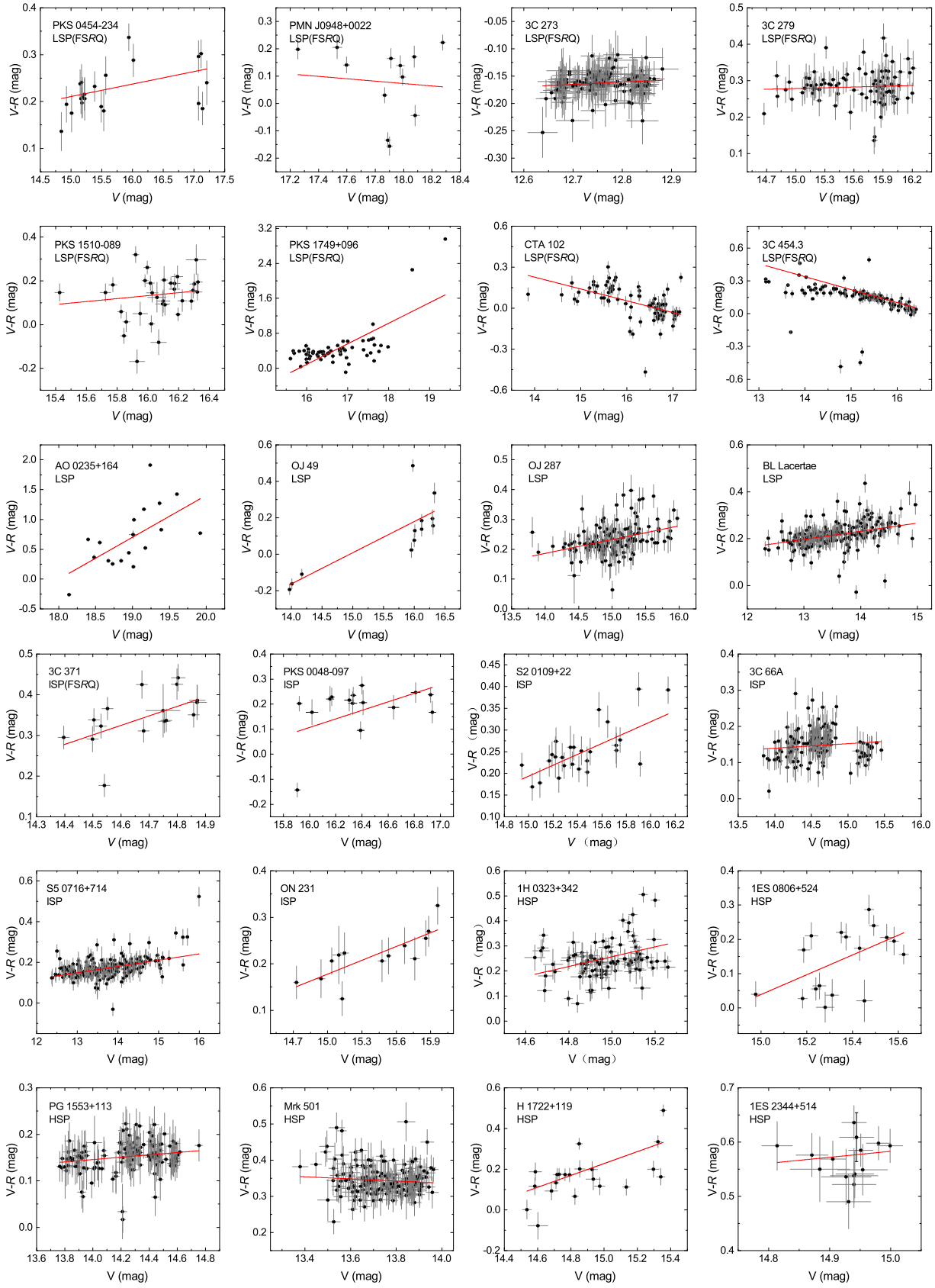

Fig. 2 $V-R$ vs. V-band magnitudes for the whole sample. In each panel, the *red solid line* represents the result of linear regression analysis.

Table 1 Summaries of our sample, linear fits to color indices $V-R$ versus V plots, average spectral index values $\langle\alpha_{VR}\rangle$ and the detected color behaviors.

Source Name	Class	ΔT (d)	$S(\sigma)$	$r(\sigma)$	P	N	$\langle\alpha_{VR}\rangle(\sigma)$	Behavior
(1)	(2)	(3)	(4)	(5)	(6)	(7)	(8)	(9)
PKS 0454–234	LSP(FSRQ)	432	0.03(0.01)	0.43(0.21)	0.052	21	1.28(0.21)	None
PMN J0948+0022	LSP(FSRQ)	394	−0.04(0.16)	−0.09(0.31)	0.786	12	0.49(0.19)	None
3C 273	LSP(FSRQ)	852	0.04(0.02)	0.15(0.08)	0.068	147	−0.93(0.19)	None
3C 279	LSP(FSRQ)	899	0.01(0.01)	0.06(0.11)	0.579	90	1.62(0.21)	None
PKS 1510–089	LSP(FSRQ)	1043	0.07(0.09)	0.14(0.18)	0.437	32	0.72(0.25)	None
PKS 1749+096	LSP(FSRQ)	907	0.47(0.06)	0.70(0.09)	$< 10^{-4}$	61	2.56(0.22)	BWB
CTA 102	LSP(FSRQ)	781	−0.09(0.02)	−0.48(0.10)	$< 10^{-4}$	84	0.23(0.22)	RWB
3C 454.3	LSP(FSRQ)	1367	−0.12(0.03)	−0.37(0.08)	$< 10^{-4}$	135	0.73(0.18)	RWB
AO 0235+164	LSP	424	0.70(0.22)	0.62(0.20)	0.006	18	3.96(0.19)	BWB
OJ 49	LSP	396	0.17(0.04)	0.83(0.18)	7.50×10^{-4}	12	0.60(0.21)	BWB
OJ 287	LSP	1260	0.05(0.01)	0.39(0.08)	$< 10^{-4}$	151	1.32(0.21)	BWB
BL Lacertae	LSP	1511	0.03(0.01)	0.37(0.06)	$< 10^{-4}$	242	1.23(0.19)	BWB
3C 371	ISP(FSRQ)	1103	0.23(0.10)	0.55(0.22)	0.03	16	1.97(0.19)	None
PKS 0048–097	ISP	368	0.17(0.09)	0.48(0.24)	0.068	15	1.04(0.23)	None
S2 0109+22	ISP	705	0.13(0.03)	0.68(0.15)	1.180×10^{-4}	26	1.43(0.19)	BWB
3C 66A	ISP	1598	0.01(0.01)	0.12(0.08)	0.132	150	0.84(0.19)	None
S5 0716+714	ISP	1367	0.03(0.01)	0.48(0.06)	$< 10^{-4}$	230	0.97(0.19)	BWB
ON 231	ISP	422	0.10(0.02)	0.81(0.18)	8.55×10^{-4}	13	1.23(0.23)	BWB
1H 0323+342	HSP	901	0.20(0.06)	0.33(0.10)	0.001	93	1.38(0.22)	BWB
1ES 0806+524	HSP	822	0.29(0.11)	0.58(0.21)	0.010	17	0.77(0.22)	BWB
PG 1553+113	HSP	904	0.03(0.01)	0.28(0.08)	0.010	148	0.87(0.20)	BWB
Mrk 501	HSP	918	−0.03(0.02)	−0.09(0.07)	0.213	179	1.96(0.21)	None
H 1722+119	HSP	900	0.29(0.08)	0.64(0.18)	0.002	21	0.95(0.22)	BWB
1ES 2344+514	HSP	645	0.11(0.22)	0.14(0.27)	0.631	15	3.21(0.24)	None

the BWB trend with $r = 0.35 \pm 0.12$ and $P = 0.008$, if considering our criteria. Furthermore, the *P*-values of several sources, e.g., 1ES 0806+524 and PG 1553+113, are just at or very close to the selection criteria, which would raise a bit of skepticism or caution. However, if we adopt and insist on the selection criteria mentioned above, it can be found that, in the sample of blazars exhibiting significant color variations with magnitudes, the BWB chromatic trend tends to appear in BL Lacs while FSRQs are more likely to follow the RWB trend.

As for the whole sample, there is a big scatter in the average spectral indices of $\langle\alpha_{VR}\rangle$, varying between -0.93 ± 0.19 and 3.96 ± 0.19. The separate distributions of $\langle\alpha_{VR}\rangle$ for BL Lac and FSRQ sources are shown in Figure 3. The mean over the entire sample (grey area) is 1.27 with a narrow distribution concentrated in the range of $0.5 \sim 1.5$. The FSQRs (green solid line) show a mean of 0.96 with one source (3C 273) displaying a negative value, while the BL Lacs (red dashed line) give a mean of 1.45 with two sources, AO 0235+164 and 1ES 2344+514, contributing values larger than 3.

It seems that the FSRQs tend to concentrate around smaller values of average spectral indices, contrary to the BL Lacs, i.e., the optical continuums of the BL Lacs in our sample are steeper than those of FSRQs, which implies strong synchrotron-dominated emission from the blazar jet and small accretion disk contribution due to relativistic Doppler-boosted jet emission (e.g., Agarwal & Gupta 2015; Gupta et al. 2017), although this (divergent) tendency is not statistically significant ($P > 0.05$) due at least partly to the small numbers in our sample, and/or some intrinsic connection between the FSRQs and BL Lacs. The distributions of $\langle\alpha_{VR}\rangle$ for LSPs, ISPs and HSPs were also investigated. The LSPs consisting of FSRQs and LSP BL Lacs show a mean of 1.15 with a broader distribution, and the ISPs and HSPs give means of 1.25 and 1.52 respectively, probably indicating an evolution of optical continuums associated with the syn-

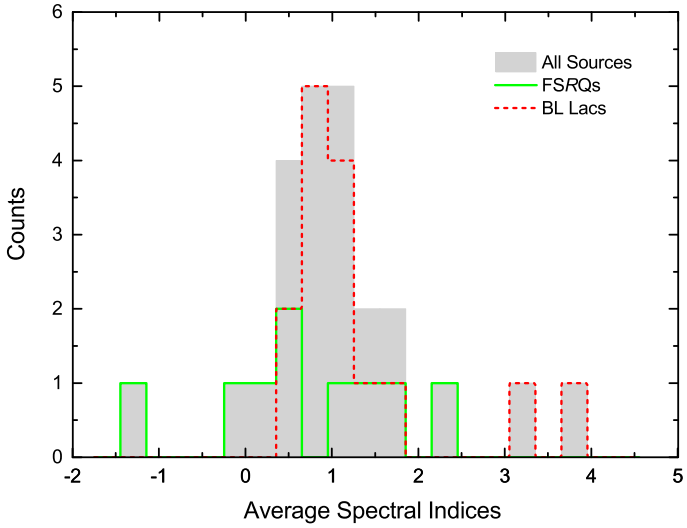

Fig. 3 Distributions of the average spectral indices $\langle \alpha_{VR} \rangle$ for BL Lacs, FSRQs and all sources. All sources (*grey area*) are shown with FSRQs (*green solid line*) and BL Lacs (*red dashed line*) superimposed.

chrotron peaks in different classes of blazars. However, such evolution seems to be statistically inconclusive due to the relatively small sample, and we also found that no significant correlation between $\nu_{\rm peak}^{\rm syn}$ and $\langle \alpha_{VR} \rangle$ can be derived from our sample.

4 DISCUSSION AND CONCLUSIONS

Color–magnitude correlations of blazars have been carried out by several authors on diverse timescales and have been seemingly associated with the blazar type: BL Lacs are often observed with a BWB trend and FSRQs usually follow an RWB trend. Vagnetti et al. (2003) reported that eight BL Lacs in their sample followed the BWB trend in the optical bands. Color–magnitude diagrams of eight red blazars over five months proposed by Gu et al. (2006) suggest that five BL Lacs showed the BWB trend, two FSRQs displayed the RWB trend and one FSRQ was achromatic. In a sample of 17 blazars, Hu et al. (2006) found that 13 BL Lacs manifested the BWB trend but four FSRQs did not follow this trend. Rani et al. (2010) reported that four in six FSRQs showed the RWB trend and three in six BL Lacs exhibited the BWB trend in their sample. Based on the Kanata observations, Ikejiri et al. (2011) found that 28 out of 32 well-observed blazars exhibited BWB trends in their entire or a part of time-series data sets and suggested that the BWB trend is universal in blazars. Zhang et al. (2015) found that 35 out of 49 FSRQs showed the RWB trend, 11 out of 22 BL Lacs exhibited the BWB trend and several blazars displayed complicated color behaviors, using the long-term optical and IR monitoring data carried out by the Small and Medium Aperture Research Telescope System (SMARTS) in Cerro Tololo, Chile. Additionally, BWB/RWB trends associated with individual BL Lac/FSRQ sources are also proposed in many diverse investigations (e.g., Raiteri et al. 2003; Hu et al. 2011; Li et al. 2015).

However, this apparent dichotomy in color variability seems to be flawed at least in some ways, due to the complicated color behavior reported by many authors. Gu & Ai (2011) found that only one FSRQ out of 29 SDSS FSRQs followed the RWB trend. Based on the SMARTS data, Bonning et al. (2012) studied 12 blazars and reported that several objects, PKS 1510–089, PKS 2215–304, OJ 287 and AO 0235+164, showed complicated and anomalous behavior rather than the dichotomy in color variability. Sandrinelli et al. (2014) found that six BL Lacs were achromatic, while all six BL Lacs in Gaur et al. (2012) exhibited the BWB trend in their sample of ten BL Lacs. Gupta et al. (2017) found that OJ 287 did not follow any significant spectral variation on long- or short-term timescales on the basis of the multi-wavelength optical photometric data, while OJ 287 in our sample did exhibit the BWB trend on long-term timescales, which is in accordance with the long-term BWB trend proposed by Zheng et al. (2008), indicating a complicated color behavior that needs to be resolved further on diverse timescales. For the long timescales, Xiong et al. (2016) suggested that Mrk 501 in different states can have different BWB trends, but this source

in our sample showed no BWB trends. Recently, using SMARTS optical/IR observations and *Fermi* γ-ray fluxes, Isler et al. (2017) argued that the color variability of 3C 279 was complicated and was difficult to reconcile with the simple RWB behavior associated with FSRQs, and suggested that the observed optical/IR color variabilities depended on a combination of the jet and disk emission.

The superpositions of a red color and an underlying blue component can be proposed to explain the apparent long-term color variations (e.g., Ikejiri et al. 2011; Agarwal & Gupta 2015; Gupta et al. 2017; Bonning et al. 2012; Gaur et al. 2012; Xiong et al. 2016; Isler et al. 2017). For the BWB trend, the constant synchrotron emission from the Doppler-boosted relativistic jet could provide the redder contribution, while the underlying blue component can be attributed to thermal emissions from the accretion disk. The RWB trend was observed probably due to a strong, blue accretion disk contribution mixed with redder jet emission, and the achromatic variations observed in blazars might be associated with different jet components becoming important in different temporal intervals (Bonning et al. 2012). Ikejiri et al. (2011) found that 3C 454.3 and PKS 1510–089 exhibited RWB trends in their faint states and BWB trends in their bright states, and suggested that the RWB trend is more likely to appear in a faint state due to the significant contribution of thermal emission from the disk, and the BWB trend in the bright state can be attributed to the dominant non-thermal jet emission. However, we did not find a significant BWB trend in their bright states based on the current data. Besides, the long-term color variations can also be interpreted as a composition of two components: a strong chromatic short-term component and a mild chromatic long-term component, which may be due to the intrinsic variations caused by particle acceleration in the jets, and the variations of the Doppler factor resulting in the shift of the observed frequency as well as the change of the flux, respectively (e.g., Raiteri et al. 2003; Gu et al. 2006; Agarwal & Gupta 2015; Gaur et al. 2015; Xiong et al. 2016, and references therein).

The complicated color behaviors associated with the abstruse emission mechanism seem to be a common feature in blazar variations. Even for one single object, different color behaviors were occasionally observed, probably due to the intrinsic mechanism and/or some kinds of selection effects, such as different bright states, time spans and flaring episodes in specific blazars. Nevertheless, in the whole sample of 24 blazars, 14 blazars showed significant color changes with magnitudes, in which 11 BL Lacs and one FSRQ exhibited the general BWB trend and two FSRQs followed the RWB tend, or four HSPs, three ISPs and five LSPs exhibited the BWB trend and two LSPs followed the RWB trend if considering the SED classification, on the long-term timescales from months to years that we concentrated on. Then, it seems possible that the trend can be derived such that BL Lacs tend to show the BWB trend while the RWB trend is especially found in FSRQs, probably consistent with BL Lacs showing dominate non-thermal emission from the jet and FSRQs having luminous accretion disks, as also evidenced by their different emission lines. The distributions of average spectral indices reveal that the optical continuums of BL Lacs are redder than those of FSRQs in our sample. The superpositions of jet and disk emission might be a possible interpretation. To investigate color behaviors more deeply and understand their physical mechanism well, dense and precise simultaneous multiwavelength observations of a much larger sample of blazars on diverse timescales are needed.

Acknowledgements This work is supported by the Education Department of Yunnan Province, China (Grant Nos. 2017ZZX079, 2016ZZX230 and 2018JS506) and the Youth Program of the Applied Basic Research Projects of Yunnan Province, China (Grant No. 2017FD147).

References

Abdo, A. A., Ackermann, M., Agudo, I., et al. 2010, ApJ, 716, 30
Agarwal, A., & Gupta, A. C. 2015, MNRAS, 450, 541
Bessell, M. S., Castelli, F., & Plez, B. 1998, A&A, 333, 231
Bonning, E., Urry, C. M., Bailyn, C., et al. 2012, ApJ, 756, 13
Böttcher, M. 2007, Ap&SS, 309, 95
Böttcher, M., Reimer, A., Sweeney, K., & Prakash, A. 2013, ApJ, 768, 54
Gaur, H., Gupta, A. C., Strigachev, A., et al. 2012, MNRAS, 425, 3002
Gaur, H., Gupta, A. C., Bachev, R., et al. 2015, MNRAS, 452, 4263
Ghisellini, G., & Tavecchio, F. 2009, MNRAS, 397, 985
Gu, M. F., Lee, C.-U., Pak, S., Yim, H. S., & Fletcher, A. B. 2006, A&A, 450, 39
Gu, M.-F., & Ai, Y. L. 2011, A&A, 528, A95
Gupta, A. C., Agarwal, A., Mishra, A., et al. 2017, MNRAS, 465, 4423

Hu, S. M., Zhao, G., Guo, H. Y., Zhang, X., & Zheng, Y. G. 2006, MNRAS, 371, 1243
Hu, S. M., Wu, J., Guo, H. Y., et al. 2011, Ap&SS, 333, 213
Ikejiri, Y., Uemura, M., Sasada, M., et al. 2011, PASJ, 63, 639
Isler, J. C., Urry, C. M., Coppi, P., et al. 2017, ApJ, 844, 107
Itoh, R., Nalewajko, K., Fukazawa, Y., et al. 2016, ApJ, 833, 77
Li, X., Zhang, L., Luo, Y., Wang, L., & Zhou, L. 2015, MNRAS, 449, 2750
Linford, J. D., Taylor, G. B., & Schinzel, F. K. 2012, ApJ, 757, 25
Lister, M. L., Aller, M., Aller, H., et al. 2011, ApJ, 742, 27
Marchesini, E. J., Andruchow, I., Cellone, S. A., et al. 2016, A&A, 591, A21
Marscher, A. P., & Gear, W. K. 1985, ApJ, 298, 114
Mücke, A., Protheroe, R. J., Engel, R., Rachen, J. P., & Stanev, T. 2003, Astroparticle Physics, 18, 593
Raiteri, C. M., Villata, M., Tosti, G., et al. 2003, A&A, 402, 151
Rani, B., Gupta, A. C., Strigachev, A., et al. 2010, MNRAS, 404, 1992
Sandrinelli, A., Covino, S., & Treves, A. 2014, A&A, 562, A79
Urry, C. M., & Padovani, P. 1995, PASP, 107, 803
Vagnetti, F., Trevese, D., & Nesci, R. 2003, ApJ, 590, 123
Wierzcholska, A., Ostrowski, M., Stawarz, Ł., Wagner, S., & Hauser, M. 2015, A&A, 573, A69
Xiong, D., Zhang, H., Zhang, X., et al. 2016, ApJS, 222, 24
Zhang, B.-K., Zhou, X.-S., Zhao, X.-Y., & Dai, B.-Z. 2015, RAA (Research in Astronomy and Astrophysics), 15, 1784
Zheng, Y. G., Zhang, X., Bi, X. W., Hao, J. M., & Zhang, H. J. 2008, MNRAS, 385, 823